Author Manuscript

Author Manuscript

Author Manuscript

Author Manuscript

HHS Public Access

Author manuscript

Proc SPIE Int Soc Opt Eng. Author manuscript; available in PMC 2014 July 28.

Published in final edited form as:

Proc SPIE Int Soc Opt Eng. 2014 March 19; 9033: 903329–. doi:10.1117/12.2043463.

High-Performance Soft-Tissue Imaging in Extremity Cone-Beam CT

W. Zbijewski[a,*], **A. Sisniega**[a], **J. W. Stayman**[a], **A. Muhit**[a], **G. Thawait**[b], **N. Packard**[c], **R. Senn**[c], **D. Yang**[c], **J. Yorkston**[c], **J. A. Carrino**[b], and **J. H. Siewerdsen**[a,b]

[a]Dept. of Biomedical Engineering, Johns Hopkins University, Baltimore, MD USA 21205

[b]Russell H. Morgan Dept. of Radiology, Johns Hopkins University, Baltimore, MD USA 21287

[c]Carestream Health Inc., Rochester NY

Abstract

Purpose—Clinical performance studies of an extremity cone-beam CT (CBCT) system indicate excellent bone visualization, but point to the need for improvement of soft-tissue image quality. To this end, a rapid Monte Carlo (MC) scatter correction is proposed, and Penalized Likelihood (PL) reconstruction is evaluated for noise management.

Methods—The accelerated MC scatter correction involved fast MC simulation with low number of photons implemented on a GPU (10^7 photons/sec), followed by Gaussian kernel smoothing in the detector plane and across projection angles. PL reconstructions were investigated for reduction of imaging dose for projections acquired at ~2 mGy.

Results—The rapid scatter estimation yielded root-mean-squared-errors of scatter projections of ~15% of peak scatter intensity for $5{\cdot}10^6$ photons/projection (runtime ~0.5 sec/projection) and 25% improvement in fat-muscle contrast in reconstructions of a cadaveric knee. PL reconstruction largely restored soft-tissue visualization at 2 mGy dose to that of 10 mGy FBP image.

Conclusion—The combination of rapid (5–10 minutes/scan) MC-based, patient-specific scatter correction and PL reconstruction offers an important means to overcome the current limitations of extremity CBCT in soft-tissue imaging.

Keywords

cone-beam CT; extremities imaging; Monte Carlo; scatter correction; nonlinear reconstruction

1. INTRODUCTION

Dedicated flat-panel detector (FPD) cone-beam CT (CBCT) [1,2] is entering clinical practice in musculoskeletal extremity imaging, where it provides a host of novel capabilities, such as weight bearing imaging. The results of a recent observer study of imaging performance of a prototype extremity CBCT unit indicated comparable overall performance with conventional multi-detector CT (MDCT), with slight preference for CBCT in bone

*wzbijewski@jhu.edu; phone 410-955-1319; fax 410-955-9826;.

Author Manuscript Author Manuscript Author Manuscript Author Manuscript

tasks and slight preference for MDCT in soft-tissue tasks. The latter is likely due to x-ray scatter (scatter-to-primary ratios of ~0.5 were found for the extremity CBCT despite the use of a grid [3]), and due to increased noise caused by the limited output of the compact CBCT x-ray source. Overcoming these limitations could enhance the potential diagnostic applications of extremities CBCT. We propose a patient-specific, Monte Carlo (MC)-based scatter correction algorithm utilizing fast MC simulations executed with low number of tracked photons and followed by kernel de-noising to yield high fidelity scatter estimates. To reduce the effects of projection noise, a penalized likelihood (PL) model-based iterative reconstructions with non-quadratic penalties and variable regularization was studied. Improvement in soft-tissue image quality was evaluated in simulations studies and clinical images of the knee.

2. METHODS

2.1 Extremities Cone-Beam CT System

The scanner (Fig. 1) involves a stationary anode x-ray tube (XRS-125-7K-P, Source-Ray, Ronkonkoma, NY) with 0.5 mm focal spot, 0.875 kW maximum power, 60–120 kVp range and added filtration of 2 mm Al + 0.2 mm Cu. No bowtie filter was used. The FPD was a PaxScan 3030+ (Varian Imaging Products, Palo Alto, CA) with a ~0.5 mm CsI:Tl operated at 25 frames/sec with 2×2 pixel binning (0.388 mm pixel pitch) and dynamic gain readout. A 10:1 antiscatter grid (Jungwon Precision Industrial, South Korea) was employed. The source-detector distance was 550 mm, source-isocenter distance was 420 mm, and the reconstruction field of view was ~22×22×22 cm^3. The system acquired 490 projections along a ~240° orbit (exceeding the half-scan range) with a scan time of 20 s. Inflatable air bladders placed inside the bore were used to reduce motion of the extremity.

2.2 Rapid Monte Carlo-Based Scatter Correction Using 3D Kernel Smoothing (MC-KS)

The flowchart of the scatter correction algorithm is shown in Fig 2. An initial reconstruction is obtained without scatter correction and segmented to provide an input to the MC simulator. The segmentation employs thresholding to classify the voxels into three materials (air, soft -tissue and bone). Within the soft-tissue and bone classes, the density of the voxels is allowed to vary as a linear function of the reconstructed attenuation in that voxel. The slopes of the associated transfer functions are determined by the nominal density of each material, as defined in the MC database, and the attenuation of the material (at nominal density) at effective beam energy. The intercepts of the transfer functions are at density equal to zero. This simple approach reduces errors that are likely to occur if e.g. all bone voxels are simulated as dense cortical bone, overestimating scatter absorption in the femur, tibia and patella. More accurate segmentation, correction and tissue modelling approaches are under investigation.

Scatter correction involved estimation of the scatter field from the segmented initial reconstruction by means of a fast Monte Carlo simulation with a low number of tracked photons. Such estimates tend to be noisy; thus kernel average smoothing was applied in 3 dimensions spanning the detector axes (u, v) and the projection angle θ to yield the following de-noised scatter estimate $S_{MC\text{-}KS}$:

Author Manuscript Author Manuscript Author Manuscript Author Manuscript

$$S_{MC-KS}(u,v,\theta)=\frac{\sum_{u_i,v_i,\theta_i}K(u,v,\theta,u_i,v_i,\theta_i)S_{MC}(u_i,v_i,\theta_i)}{\sum_{u_i,v_i,\theta_i}K(u_i,v_i,\theta_i)} \quad (1)$$

where S_{MC} is the noisy initial MC scatter estimate, K is a 3-dimensional Gaussian kernel acting on the distance between two points in the (u, v, θ) space, and index i runs through all points in the scatter singoram. The de-noised scatter estimates $S_{MC\text{-}KS}$ were subsequently subtracted from the measured projections, and a corrected reconstruction was computed. Note that the sinogram locations where the scatter estimate is computed (u, v, θ) do not need to coincide with the locations where the MC data is available (u_i, v_i, θ_i), allowing for application of this methodology to scenarios where MC simulation is performed only for a subset of projection angles or detector cells.

Earlier studies demonstrated that 3-dimesional iterative Richardson-Lucy (RL) [4] de-noising effectively exploits the smoothness of scatter fields in u, v and θ to provide 3–4 orders of magnitude acceleration over plain MC. By replacing the RL fitting with kernel smoothing, we investigate a simpler de-noising algorithm that is non-iterative, and thus potentially more efficient.

MC was implemented on a GPU [5] (Nvidia GTX 780 Ti GPU with 2880 CUDA cores and 3 GB on-board memory, Nvidia, Santa Clara, CA) to provide basic acceleration through massive parallelism, achieving simulation times of 1×10^7 photons/sec for a knee. The MC system model included polyenergetic x-ray spectra and analytical models of a CsI:Tl FPD and the 10:1 anti-scatter grid [3]. MC-KS was tested in simulated 80 kVp (+2 mm Al, +0.2 mm Cu) projections of a knee from the Virtual Population dataset (www.itis.ethz.ch). The phantom was segmented into 7 tissues at 1 mm voxel size; 240 reference primary projections were computed (1° steps) with polyenergetic forward projector. Reference scatter projections were obtained with MC with ~10^{11} photons/frame; both simulations used the detailed extremity CBCT model described above. Real data tests of MC-KS utilized projections of a cadaveric knee obtained on a CBCT imaging bench emulating the geometry of the scanner (80 kVp+0.2 mm Cu, +2 mm Al, 240 projections, 120 mAs total) with the 10:1 antiscatter grid.

2.4 Noise Reduction With PL

Iterative reconstruction was studied with the separable paraboloidal surrogates PL algorithm [6] applied to projections of a cadaveric knee obtained on the prototype system using the nominal 80 kVp, 10 mGy protocol described in **Sec. 2.1**, as well as a reduced dose 80 kVp protocol at 2 mGy (20 mAs). The Huber function penalty was employed with varied penalty strength β and quadratic neighbourhood size δ. Increasing β corresponds to stronger blur; increasing δ extends the threshold below which the data is quadratically penalized and above which a total-variation penalty is applied. Ordered subsets acceleration was applied with 5 projections/subset.

Author Manuscript Author Manuscript Author Manuscript Author Manuscript

3. RESULTS AND BREAKTHROUGH WORK

Fig. 3 and 4 illustrate the performance of the prototype extremities CBCT unit compared to MDCT for bone and soft-tissue imaging tasks, respectively. Fig. 3(A) demonstrates the high resolution of the CBCT unit in imaging of a bone cyst. High quality bone visualization, combined with simplified logistics compared to MDCT and a favorable dose profile enable novel imaging applications on the extremities CBCT, such as longitudinal studies of fracture healing performed as a part of the ongoing clinical pilot study and illustrated in Fig. 3(B). While the performance of the CBCT system in bone imaging tasks is often superior to MDCT, the visualization of soft tissues is approaching that of MDCT, but could benefit from further refinement. This is illustrated in Fig. 4 in a comparison of soft-tissue MDCT and CBCT imaging of the knee. Possible limitations of CBCT in soft-tissue tasks include scatter artifacts, seen here in the Hoffa fat pad (arrow), and increased noise (due to limited tube power) compromising assessment of the continuity of soft-tissue structures in CBCT (also marked with arrow). This motivates the studies of MC scatter correction and PL noise reduction.

In Fig. 5 the low noise reference scatter projections of a digital knee phantom [one projection angle form the reference dataset is shown in Fig. 5(A)] are compared with the results of kernel smoothing applied to noisy scatter estimates obtained with fast simulations at $5{\cdot}10^6$ – 10^8 photons/frame. In Fig. 5(B), the root mean squared error (RMSE) computed vs. the reference scatter distribution across the complete range of projections is shown for MC-KS with varying sizes of the Gaussian smoothing kernel σ (isotropic in u, v and θ).

In Fig. 5(C), the noisy initial MC estimate with low number of photons (top row), are compared to the result of MC-KS de-noising (bottom row) using σ selected to yield minimal RMSE as in Fig. 5(B). The same projection angle as for the reference MC estimate in Fig. 5(A) is shown. RMSE of MC-KS is reduced with increasing number of simulated photons (decreasing noise in the scatter estimates). The size of the smoothing kernel yielding minimal RMSE decreases with increasing number of tracked photons, illustrating the trade-off between errors due to kernel blur and due to noise in the initial scatter estimates. Comparison of MC-KS with the reference scatter projection shows high fidelity and only slight pattern noise due to the smoothing kernel even for MC-KS estimates obtained at $5{\cdot}10^6$ – 10^7 photons/frame (simulation times of ~1 sec/frame).

Fig. 6 illustrates the performance of MC-KS (using KS kernels optimized in Fig. 5) in a cadaveric knee. Reconstruction of projections obtained with 2 cm collimation (and thus significantly reduced scatter) is compared to one acquired with full field-of-view (FOV), demonstrating the magnitude of scatter artifacts. In addition to MC-KS, scatter correction was also performed assuming constant scatter per projection, where the magnitude of scatter was obtained as a fixed fraction of the mean projection pixel value in an ROI at the center of the detector. The value of the scatter fraction was estimated based on the MC scatter simulation with 10^8 photons/frame (“oracle” scatter fraction correction). Improvements in the uniformity of the image (seen e.g. in the fat areas indicated with arrows) and in the reconstructed bone attenuation (also indicated with an arrow) are demonstrated in the comparison of MC-KS with the collimated acquisition and the uncorrected full FOV data.

Author Manuscript Author Manuscript Author Manuscript Author Manuscript

Compared to the “oracle” scatter fraction correction, MC-KS attains better overall agreement with the narrow beam reconstruction in terms of reconstructed attenuation values. No apparent bias is introduced even for the MC-KS with $5 \cdot 10^6$ photons (~0.6 sec/projection). Fig. 7 further illustrates the performance of MC-KS scatter correction in a sagittal view of the cadaveric knee. Reduction of shading artifacts is visible in this plane e.g. in the improved uniformity of deep and superficial fat layers in MC-KS reconstructions compared to uncorrected volume and “oracle” correction. Contrast (C) and Contrast-to-Noise ratio (CNR) in fat and muscle regions indicated with blue dashed boxes in Fig. 6 are listed in Table 1. Contrast is reduced by 25% due to scatter, with similar reduction in Contrast-to-Noise ratio (CNR). When MC-KS scatter correction is applied to the full FOV data, the contrast is restored and even slightly (7–10%) increased compared to the narrow beam data. With the “oracle” scatter fraction correction, the contrast remains reduced by approx. 15% compared to the narrow beam data. Note that the gain in CNR is not as significant as the gain in contrast due to the remaining scatter noise in the scatter-corrected projections.

Noise reduction in CBCT can be achieved through PL reconstruction, which explicitly models projection noise and applies flexible regularization to optimize resolution-noise tradeoff, as illustrated in Fig. 8. FBP reconstruction using nominal soft-tissue Hann filter and the nominal imaging dose of 10 mGy is compared to FBP reconstruction with the same filter obtained at 2 mGy and PL reconstruction of the low-dose data with varied β and δ, with β selected to approximately match the resolution of the FBP image (assessed at the tendon marked with arrow). PL restores the visibility of soft-tissue in the 2 mGy scan to approximately that of the 10 mGy FBP reconstruction, as shown e.g. by the improved continuity of the tendon and improved visualization of an air pocket (arrows).

4. CONCLUSIONS

Observer tests confirm a slight preference for CBCT in bone imaging, and a slight preference for MDCT in soft-tissue visualization due to increased scatter and noise in CBCT. A rapid MC-based scatter correction strategy based on kernel smoothing was shown to achieve significant reduction of scatter artifacts and 25% improvement in contrast with MC simulation times of only ~0.5 sec per projection (~5 mins/scan) on a modest GPU (NVIDIA GTX 780). Further acceleration is expected through MC variance reduction techniques [3]. PL reconstruction was investigated for improving noise-bias tradeoff in extremity CBCT (including reduction of uncorrected noise from scatter). Initial visual assessment confirmed improved soft-tissue visualization and potential for further dose reduction in CBCT with PL, with numerical assessment of image quality underway. The soft-tissue image quality improvements described here, combined with the novel ability to image weight-bearing extremities and advantages in patient comfort and logistics are likely to establish CBCT as a compelling alternative to MDCT in a broad scope of extremity imaging applications.

Acknowledgments

Work supported by NIH Grant No. 2R01-CA-112163, R21-AR-062293, and Carestream Health.

Author Manuscript Author Manuscript Author Manuscript Author Manuscript

References

1. Carrino JA, Muhit A, Zbijewski W, Thawait GK, Stayman JW, Packard N, Senn R, Yang D, Foos DH, Yorkston J, Siewerdsen JH. Dedicated Cone-Beam CT System for Extremity Imaging. Radiology. 2014; 270(3):816–24. [PubMed: 24475803]
2. Tuominen EK, Kankare J, Koskinen SK, Mattila KT. Weight-bearing CT imaging of the lower extremity. AJR Am J Roentgenol. 2013; 200(1):146–148. [PubMed: 23255755]
3. Sisniega A, Zbijewski W, Badal A, Kyprianou IS, Stayman JW, Vaquero JJ, Siewerdsen JH. Monte Carlo study of the effects of system geometry and antiscatter grids on cone-beam CT scatter distributions. Med Phys. 2013; 40(5):051915. [PubMed: 23635285]
4. Zbijewski W, Beekman FJ. Efficient Monte Carlo based scatter artifact reduction in cone-beam micro-CT. IEEE Trans Med Imaging. 2006; 25(7):817–27. [PubMed: 16827483]
5. Badal A, Badano A. Accelerating Monte Carlo simulations of photon transport in a voxelized geometry using a massively parallel graphics processing unit. Med Phys. 2009; 36(11):4878–80. [PubMed: 19994495]
6. Erdoğan H, Fessler JA. Monotonic algorithms for transmission tomography. IEEE Trans Med Imaging. 1999; 18(9):801–14. [PubMed: 10571385]

Author Manuscript Author Manuscript Author Manuscript Author Manuscript

Figure 1.
The extremity CBCT unit currently in clinical pilot studies in a standing configuration for imaging of weight-bearing lower extremities in natural stance and in a sitting configuration for imaging of lower and upper extremities

Author Manuscript Author Manuscript Author Manuscript Author Manuscript

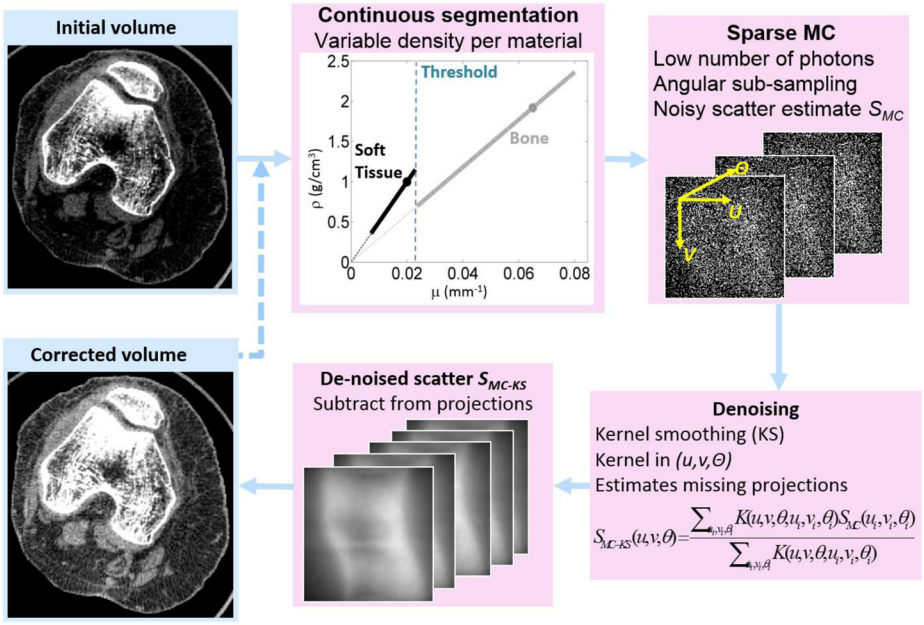

Figure 2.

Flowchart of the rapid MC-based scatter correction algorithm involving fast MC scatter estimation with low number of photons followed by denoising via kernel smoothing with 3D Gaussian kernels extending in the projection plane and across projection angles.

Author Manuscript Author Manuscript Author Manuscript Author Manuscript

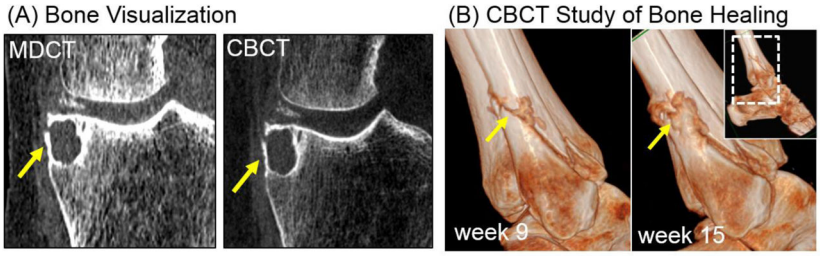

Figure 3.

(A) Bone visualization in MDCT and CBCT for a knee joint with a bone cyst (arrow). (B) CBCT study of fracture healing.

Author Manuscript Author Manuscript Author Manuscript Author Manuscript

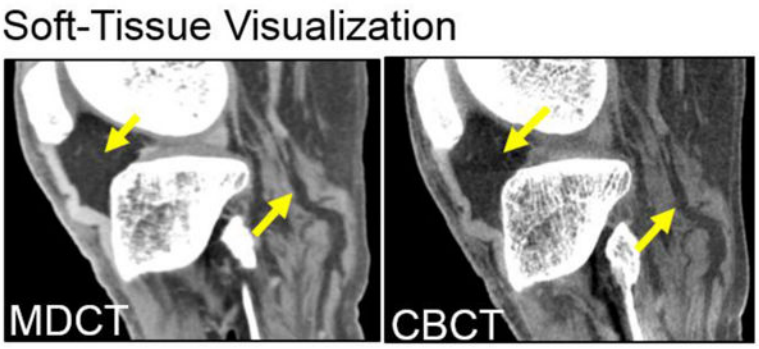

Figure 4.
Soft-tissue visualization in a knee.

Author Manuscript Author Manuscript Author Manuscript Author Manuscript

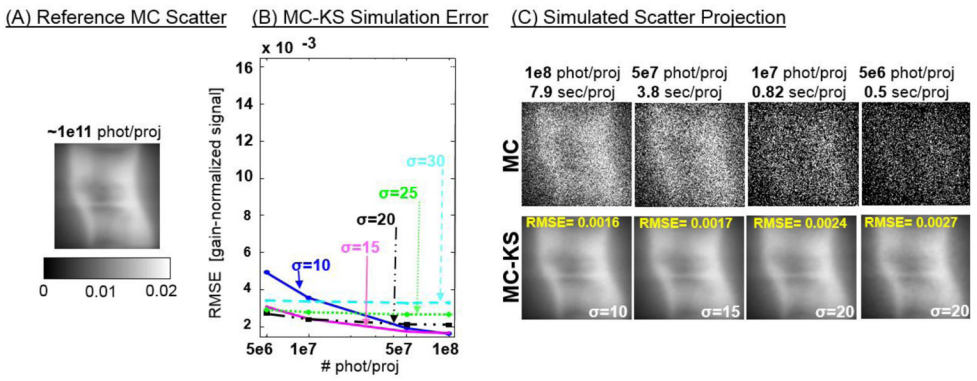

Figure 5.

(A) Reference scatter projection obtained with a large number of simulated photon tracks. (B) RMSE of MC-KS vs. the reference scatter projections of a knee phantom as a function of the number of photons in the MC-KS simulation and the size of the isotropic smoothing kernel σ. (C) MC estimates obtained with low number of tracked photons and the results of kernel smoothing with optimal kernels found in (B).

Author Manuscript Author Manuscript Author Manuscript Author Manuscript

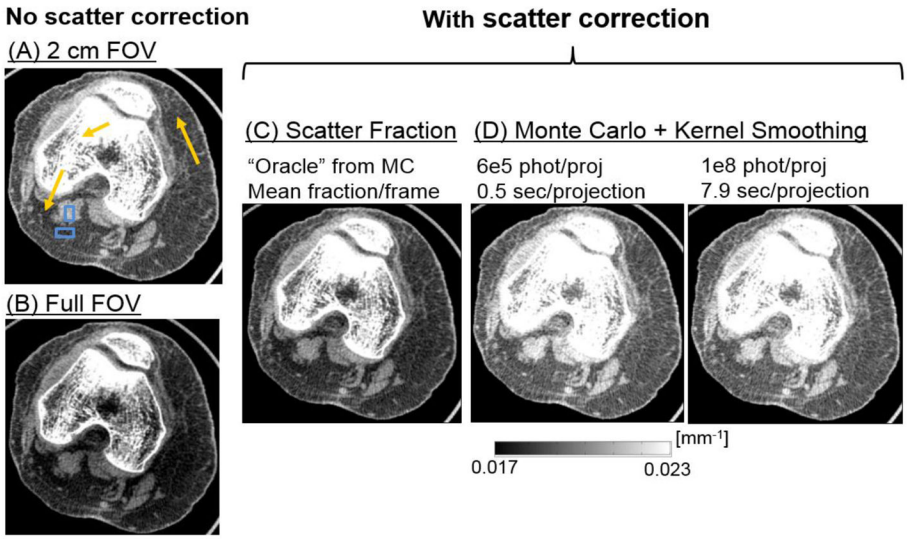

Figure 6.

Scatter correction for an axial slice through a cadaveric knee. **(A)** Narrow beam reconstruction. **(B)** Uncorrected full FOV reconstruction. **(C)** Full FOV reconstruction with "oracle" scatter fraction correction. **(D)** MC-KS scatter correction with $5{\cdot}10^6$ photons/frame and KS kernel σ=20 (as optimized in Fig. 5 and MC-KS scatter correction with $1{\cdot}10^8$ photons/frame and KS kernel σ=10.

Author Manuscript Author Manuscript Author Manuscript Author Manuscript

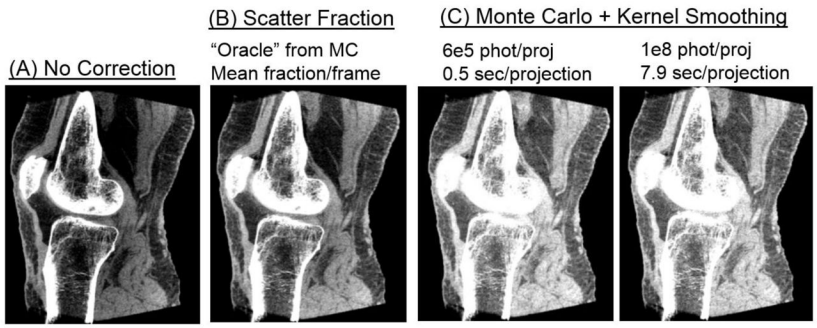

Figure 7.
MC-based scatter correction illustrated in a sagittal view of a cadaveric knee.

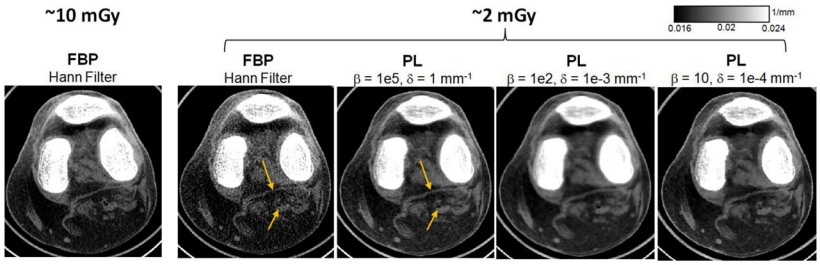

Figure 8.

Noise reduction through PL reconstruction. FBP reconstruction at nominal dose is compared to FBP and PL reconstructions at 5-fold reduced dose for varied parameters of the PL penalty.

Author Manuscript Author Manuscript Author Manuscript Author Manuscript

Author Manuscript Author Manuscript Author Manuscript Author Manuscript

Table 1

Contrast and contrast-to-noise (CNR) in reconstructions of the cadaveric knee with and without scatter correction

	No scatter correction		With scatter correction		
	2 cm FOV	Full FOV	Scatter fraction	MC-KS, 6e5 phot/proj	MC-KS, 1e8 phot/proj
Contrast [mm^{-1}]	0.0029	0.0022	0.0025	0.0032	0.0031
CNR	6.38	5.69	5.97	5.69	6.06